JOURNAL OF AIRCRAFT
Vol. 41, No. 4, July–August 2004

Durability Characterization of Active Fiber Composite Actuators for Helicopter Rotor Blade Applications

Viresh K. Wickramasinghe*
Institute for Aerospace Research, National Research Council Canada, Ottawa, Ontario, Canada, K1G 0R6
and
Nesbitt W. Hagood†
Continuum Photonics, Inc., Billerica, Massachusetts 01821

Theprimary objective of this work was to characterize the long-term durability performance of the Active Fiber Composite (AFC) actuator material system for the Boeing Active Material Rotor (AMR) blade application. The AFCs were a new structural actuator system consisting of piezoceramic fibers embedded in an epoxy matrix and sandwiched between interdigitated electrodes. These actuators were integrated directly into the blade spar as active plies within the composite structure to perform structural actuation for helicopter vibration control. Therefore, it was necessary to conduct extensive electromechanical material characterization to evaluate AFCs both as actuators and as structural components of the blade. The long-term durability characterization tests designed to extract important electromechanical properties were electrical fatigue tests and mechanical fatigue tests. This paper presents the test results as well as the comprehensive testing process developed to evaluate the relevant AFC durability properties. The durability tests conducted under simulated electromechanical loading conditions expected on AFCs during the blade operation provided an invaluable insight into the behavior of the AFCs under dynamic loading environment. The results from this comprehensive durability characterization of the AFC material system supported the design and operation of the Boeing AMR blade scheduled for wind tunnel tests.

Introduction

SIGNIFICANT structural vibration due to unsteady aerodynamics in the rotor blade environment is a notable and undesirable characteristic of helicopter flight.[1] The rotor vibration transferred throughout the helicopter structure contributes to poor ride quality for passengers, fatigue of expensive structural components, and high acoustic signature for the vehicle. In addition to passive approaches, such as vibration absorbers, active control solutions are currently being investigated to suppress the rotor vibration. The individual blade control (IBC) approach has been identified as one of the most promising methods under current development. IBC places actuators on each blade to actively control the aerodynamic loads on the blade independently and simultaneously to suppress rotor vibration at the source.[2]

IBC has been implemented using two distinct actuation concepts, namely, discrete and integral. The discrete actuation concept employs a blade embedded actuator to control a trailing edge servoflap. In 1999, a one-sixth-scale blade with a trailing-edge flap based on an X frame displacement amplification concept, driven by a stacked piezoelectric actuator, was developed and hover tested by Prechtl and Hall.[3] A full-scale version, the double X frame, is to be incorporated on an MD-900 rotor blade for flight tests by Boeing Helicopters.[4]

In the integral actuation concept, the actuator system is embedded into the blade skin along the span to obtain a smooth continuous structural deformation. In 1998, Rodgers and Hagood developed an integrally actuated one-sixth-scale CH-47D blade, which was tested in hover.[5] A set of Froude-scale active-twist blades was built and tested by Shin and Cesnik.[6] The actuator system used in the preceding projects was known as active fiber composite (AFC). The AFCs were a new actuator material system consisting of piezoceramic fibers embedded in an epoxy matrix that were integrated directly into the blade spar laminate as active plies within the composite structure. This distributed 45-deg actuator system twisted the blade structure to vary the angle of attack to induce aerodynamic loads necessary to suppress rotor vibration effectively.[7] In addition, actively controlled blades may also increase the helicopter payload and cruise speed.[8] However, only a few AFC material characterization studies have been conducted.[9,10]

This paper focuses on the long-term durability characterization of a new AFC actuator material system embedded in the Boeing active material rotor (AMR) blade manufactured in Phase II of the Smart Materials and Structures Demonstration Consortium. The AMR was a set of one-sixth-scale, Mach-scaled, advanced CH-47 blades scheduled for hover and forward flight wind-tunnel tests.[11] The swept tipped AMR blade manufactured for the wind-tunnel test and a sample of the 45-deg AFC actuators distributed along the blade are shown in Fig. 1. The blade consisted of 15.5-mm-thick composite D-spar and an aerodynamic fairing. Four active plies, each consisting of six 45-deg AFCs, were embedded in the top and the bottom of the spar laminate to provide integral twist actuation. The total blade radius was 1.5 m and the active length was 1 m. The high voltage necessary to actuate the AFCs was supplied through a flexible circuit within the composite laminate, as seen in Fig. 1. This integral actuation technology continues to be developed by Boeing Helicopters.[12]

Because the AFC was a new and unique actuator material system, it was necessary to extensively modify existing test procedures, where they existed, and to develop new test procedures to extract the important electromechanical properties. The uniqueness of the

Received 4 March 2003; presented as Paper 2003-1511 at the AIAA/ASME/ASCE/AHS 44th Structures, Structural Dynamics, and Materials Conference, Norfolk, VA, 7 April 2003; accepted for publication 12 June 2003.

*Research Assistant, Active Materials and Structures Laboratory; formerly with the Massachusetts Institute of Technology, Cambridge, Massachusetts. Research Associate, Structures, Materials, and Propulsion Laboratory, Institute for Aerospace Research, U-66A Uplands Drive, National Research Council Canada, Ottawa, Ontario, K1G 0R6, Canada. Member AIAA.

†Assistant Professor, Department of Aeronautics and Astronautics; formerly with the Massachusetts Institute of Technology, Cambridge, Massachusetts. Chief Technology Officer, 5 Fortune Drive, Continuum Photonics, Inc., Billerica, MA 01821.

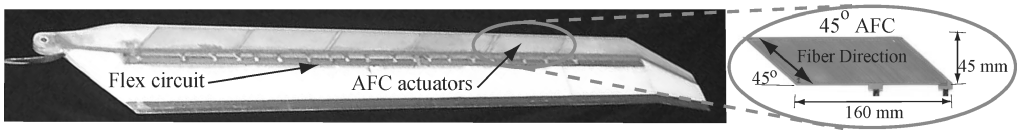

Fig. 1 Boeing AMR blade and a 45-deg AFC bade actuator.

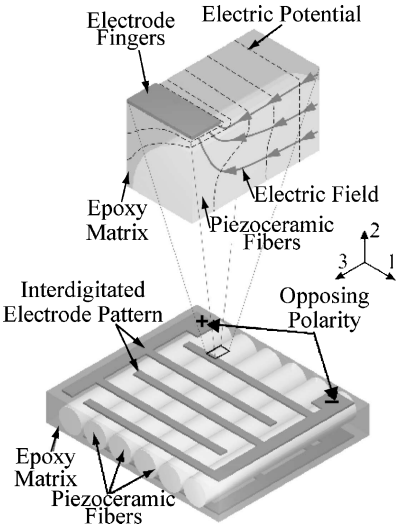

Fig. 2 Schematic of an AFC.

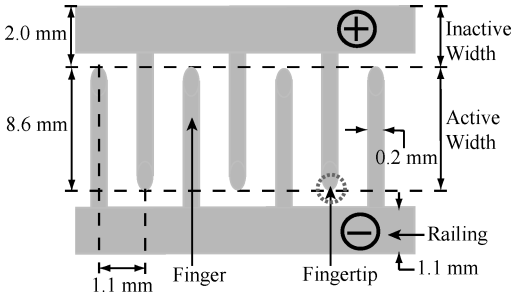

Fig. 3 Interdigitated electrode pattern.

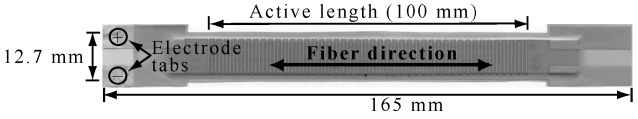

Fig. 4 Baseline 0-deg AFC actuator test coupon.

material characterization requirements stemmed not only from the structural actuation capability of AFCs but also from that AFCs were used as hybrid lamina incorporated as active plies within the composite blade structure. Therefore, extensive material characterization was necessary to evaluate AFCs as actuators and as structural components of the blade. Important material performance properties and long-term durability properties of the AFC material for the AMR blade application were identified, and comprehensive testing methodologies were developed to extract the relevant properties under simulated blade operating conditions. The primary objective of this paper is to characterize the long-term durability performance of the AFC actuator material system by subjecting the AFCs to electrical fatigue and mechanical fatigue environments. In the past, there have been only a few durability studies performed on piezoceramic embedded composites.[13] The basic AFC material performance properties extracted from stress–strain tests, free strain tests, and actuation under tensile load tests have been published.[14]

AFC Actuator Material System

The AFC actuator material system used continuous piezoceramic fibers, which were aligned to provide in-plane actuation due to the inherent electrical and mechanical coupling characteristic.[15] A mechanical displacement of the piezoceramic material generated an electric field, and the reverse process was also true. An application of an electric field caused a mechanical deformation in the material, resulting in a significant mechanical force that could be used for structural actuation.[16,17] The AFC material system characterized for the AMR blade application included 0.25-mm-diam PZT-5A fibers (CeraNova Corporation, Franklin, Massachusetts). The fibers were manufactured through an extrusion process using a mixture of PZT-5A powders.[18]

The piezoceramic fibers were aligned in an epoxy matrix as shown in Fig. 2. These ceramic fibers with high stiffness provided the actuation authority, but the fibers tended to crack at relatively low mechanical strains due to their brittle nature. However, the strength and toughness properties of the AFC actuator were significantly improved due to the polymer matrix that surrounded the fibers. For example, the onset of macroscopic fiber damage on AFCs was observed above 2500 $\mu\varepsilon$ (Ref. 14) even though the nominal tensile fracture strain of PZT-5A bulk material was only 1250 $\mu\varepsilon$ (Ref. 19). The polymer matrix material provided a path for an efficient load transfer around cracked fibers, which allowed the actuator to withstand higher mechanical strains than individual fibers. Furthermore, the matrix helped to prevent a crack in a fiber from propagating to adjacent fibers, thereby inhibiting macroscopic damage in the AFC at high mechanical strains. This was an improvement over actuators based on piezoceramic wafers, which are prone to macroscopic and catastrophic damage resulting from cracks in the wafer at very low strains.[20]

The piezoceramic fibers embedded in the matrix were sandwiched between two layers of polyimide film that had a conductive interdigitated electrode pattern printed in the inner surface. The voltage applied through the interdigitated electrode oriented the electric field along the fibers to actuate the AFC using the primary piezoceramic effect, d_{33}, for optimum actuation.[21] Therefore, an application of an excitation voltage to the actuator caused an in-plane mechanical deformation in the direction of the fibers. The details of the electrode pattern used in the material characterization test coupons are shown in Fig. 3. The interdigitated electrode was printed with silver ink on 25.4-μm Kapton substrate. The electrode fingers were 0.2 mm wide and 1.1 mm apart. The electrode railings were 1.1 mm wide, which connected the appropriate electrode fingers to the electrode tab with the correct polarity. The interdigitated electrode pattern created an active width in the middle of the actuator and an inactive width on each side, as shown in Fig. 3. The electrode fingers with both polarities were in the active width to provide an effective electrical field, whereas the inactive width had electrode fingers with only one polarity. As a result, the high stiffness ceramic fibers left in the inactive area during the manufacturing process act as a constraint to the actuator, lowering the induced actuation strain performance.

The 0-deg actuator coupon design used for durability characterization tests is shown in Fig. 4. These 0-deg test coupons closely represented the actuator material configuration of the 45-deg AMR blade actuators. The active length was 100 mm. The active length was defined as the distance between the edge electrode fingers at each end of the interdigitated pattern. The average thickness of a baseline AFC coupon was 0.34 mm, and ~90% of the active width was filled with fibers as in Fig. 5, similar to the AMR blade actuators. The AFCs were poled in air at 100°F with 4000 Vdc for 20 min to enhance the actuation. Because the AFC material properties were highly dependent on the manufacturing process, all of the actuators used in this durability characterization study were manufactured

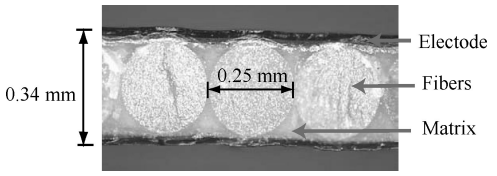

Fig. 5 Cross section of AFC actuator.

by the vendor (Continuum Control Corporation, Billerica, Massachusetts) for the blade actuators.

Electrical Fatigue Tests

The electrical fatigue tests were designed to simulate the repeated high-frequency actuation of AFCs during the AMR blade operation. It was important to determine the ability of the AFC to actuate reliably for long durations while sustaining its induced strain performance. The repeated actuation at high frequencies could lead to degradation in the actuator performance, heating of the actuator, or even catastrophic electrical failure within the actuator material system. Therefore, electrical fatigue tests were used to characterize the long-term durability of AFCs under high-frequency actuation conditions.

In electrical fatigue tests, the actuators were cycled to 20 million cycles using a 3000-Vpp (voltage peak-to-peak) sinusoidal driving voltage with 0 Vdc, the highest driving voltage expected in the AMR blade operation. The ideal fatigue frequency was 100 Hz because it would be the highest actuation frequency used in the AMR blade operation. However, some of the tests were conducted at 200-Hz frequency to accelerate these time-consuming tests. The total durations for a 20 million cycle fatigue test at 100 and 200 Hz were 60 and 30 h, respectively.

Test Articles

The narrow actuator coupons shown in Fig. 4 were used for electrical fatigue tests. Four baseline coupons were tested to facilitate inspection of piezoceramic fibers inside the actuator using a microscope to detect any damages. Two actuators were symmetrically laminated with two plies of E120 (Hexcel Corporation, Pleasanton, California) E–glass woven fabric (2 E120) to simulate the constraint condition expected in the AMR blade due to the surrounding passive composite structure. This E120 fabric was a [0-deg/90-deg] cross ply prepreg E–glass fabric. Also note that half of the test specimens had extra piezoelectric fibers to have fibers underneath the electrode fingertips. It was expected that having fibers underneath the electrode fingertips increased the vulnerability of AFCs to electrical fatigue damage. This configuration simulated the AMR blade actuators. Because of manufacturing limitations, one edge of the blade actuators would always have fibers underneath the electrode fingertips.

Test Setup and Procedure

The electrical fatigue test apparatus was designed to measure actuator-induced strain while minimizing undesired external loads, such as frictional loads. The AFC was placed horizontally on a custom fabricated Plexiglas® test rig shown in Fig. 6, and the surface was covered with guaranteed nonporous Teflon® tape to minimize friction between the actuator and the test rig surface. One end of the actuator was fixed by clamping it to the test rig, while the other end was allowed to move freely. A pair of guides was placed along the edges of the AFC to minimize out-of-plane movement during the actuation process.

The test rig was installed on an optical table, and actuation strain was measured using the ZMI-1000 (Zygo Corporation, Middlefield, Conneticut) laser displacement measuring interferometer system. A retroreflector was attached to the free end of the actuator as a target to reflect the measurement laser beam back to the interferometer system. The high-voltage sinusoidal electrical signal required to actuate the AFC was supplied using a 10-kV high-voltage amplifier (Trek, Inc., Medina, New York) and a function generator. The LabVIEW (National Instruments Corporation, Austin, Texas) data acquisition

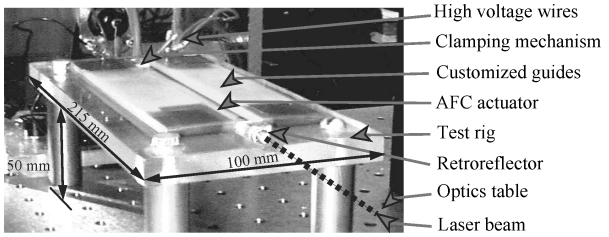

Fig. 6 Test setup for electrical fatigue tests.

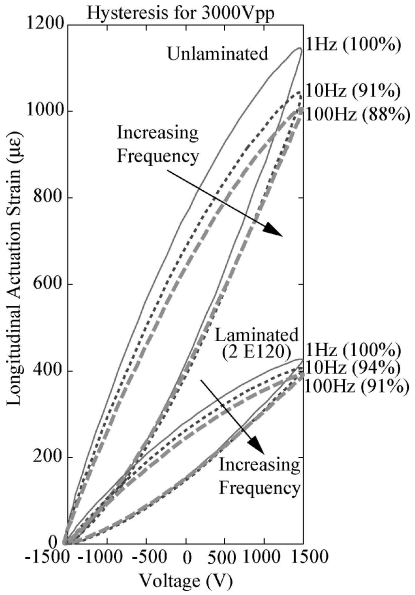

Fig. 7 AFC hysteresis behavior.

software recorded actuator displacement and applied voltage. The actuation strain was calculated through normalizing the actuator displacement measured by the laser interferometer system using the active length of 100 mm.

In addition, a type K thermocouple was attached to the actuator surface to monitor heating due to repeated actuation. During the test, the induced strain of the actuator was measured at logarithmic electrical cycle intervals to identify variation in actuator performance. Also, at less frequent intervals, the actuators were inspected using a microscope to detect damage within the actuator that could not be observed with the naked eye. Microscopic inspection enabled the detection of fatigue burns that might occur in the AFC material due to repeated high-frequency actuation.

Test Results

The sinusoidal voltage applied to the AFC produced a nonlinear hysteretic behavior of voltage and actuation strain as typically observed with piezoceramic actuators. The hysteresis observed on an unlaminated baseline actuator and an actuator symmetrically laminated with two plies of E–glass operated with 3000-Vpp + 0 Vdc at 1, 10-, and 100-Hz frequencies are shown in Fig. 7. Laminating the AFC with E–glass added elastic constraint to the actuator, and symmetrical lamination with two plies of E–glass decreased the actuation strain by ~65%. The test conditions and the initial actuator performance for each specimen used for electrical fatigue tests are summarized in Table 1. Note that specimens B39, B40, and B41 were manufactured with extra fibers underneath the electrode fingertips. The addition of fibers outside the active area increased the stiffness of the inactive area and, consequently, reduced the induced strain performance of the AFC actuator significantly.

To compare the performance variation among samples during the electrical fatigue test, the induced strain output for each coupon was normalized by the initial actuation at the fatigue frequency. The variation in normalized actuator performance with the number of electrical cycles is shown in Fig. 8. All actuators survived

Table 1 Summary of electrical fatigue specimens and test conditions

Specimen	E–glass lamination	Fatigue frequency, Hz	Initial actuation, $\mu\varepsilon$
B25	None	100	1064
B39	None	100	613
B26	None	200	1047
B40	None	200	623
B47	2 E120	200	523
B41	2 E120	200	326

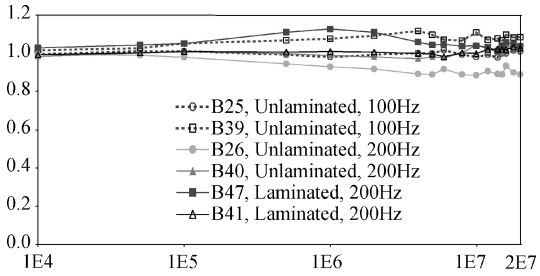

Fig. 8 Actuation performance variation during electrical fatigue tests.

the electrical fatigue test to 20 million cycles with no significant heating during the test. The actuator temperature measured using the thermocouple was within 5°F above ambient room temperature. The induced strain performance of five out of a total of six actuators showed scatter in performance during the test, but no continuous degradation in actuation was observed. Only one actuator, B26, showed a continuous deterioration in performance, retaining 85% of the initial performance at the end of 20 million cycle test.

However, detailed inspection of the unlaminated baseline test specimens after 1 million electrical cycles showed evidence of microscopic damage in the form of fatigue burns. The locations of the detected burns were marked on the actuator, and the same burn sites were observed repeatedly at logarithmic cycle intervals during the test to evaluate their growth.

Specimens B25 and B26, which had no fibers underneath electrode fingertips, showed approximately 20 microscopic burn sites along a few of the electrode fingers. These electrical fatigue burns were observed on piezoceramic fiber surfaces closest to the electrode finger and grew slowly along the same finger during the test. The time histories of two of the burns from specimen B25 and B26 are shown in Fig. 9. It was observed that fatigue burns did not tend to grow from one electrode finger to the adjacent finger with the opposite polarity, but the burn extended along the edge of the same electrode finger.

Both B39 and B40 specimens were manufactured with extra piezoelectric fibers to place some fibers under electrode fingertips. Microscopic inspection detected few fatigue burns along the electrode fingers that were similar to B25 and B26. However, it was observed that most burns occurred on the fibers underneath the electrode fingertips. The burns along the electrode fingers showed little growth, whereas those at the fingertips grew considerably during the test. The growth histories of two burns observed on electrode fingertips in specimens B39 and B40 are shown in Fig. 10. This may be due to higher concentration of electrical charge in the electrode fingertips due to its geometry, which consequently made those locations more prone to electrical fatigue damage.

The E–glass laminated specimens, B41 and B47, did not show any fatigue burns severe enough to be visible through the layers of E–glass.

Note that, during the 20 million cycle test, none of these fatigue burns extended a significant distance away from the electrode finger. Catastrophic failure of the actuator could have been caused if the burn reached the adjacent electrode finger with the opposite polarity. One possible explanation for the fatigue burn phenomenon could be charring of the matrix material due to high-current flow between the fiber surface and the electrode finger. The high currents were

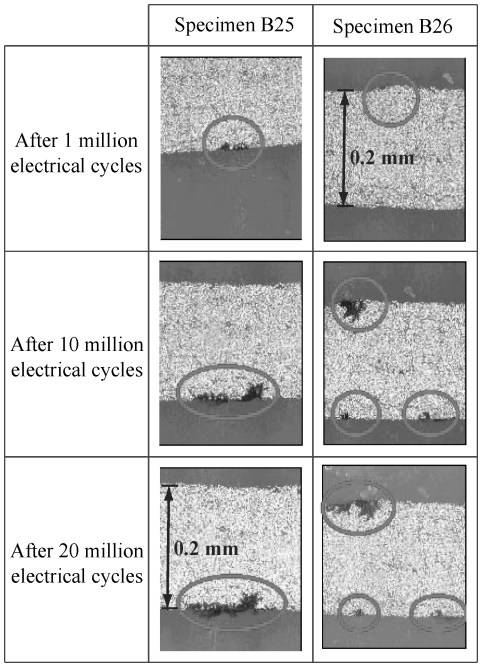

Fig. 9 Electrical fatigue burns along electrode fingers.

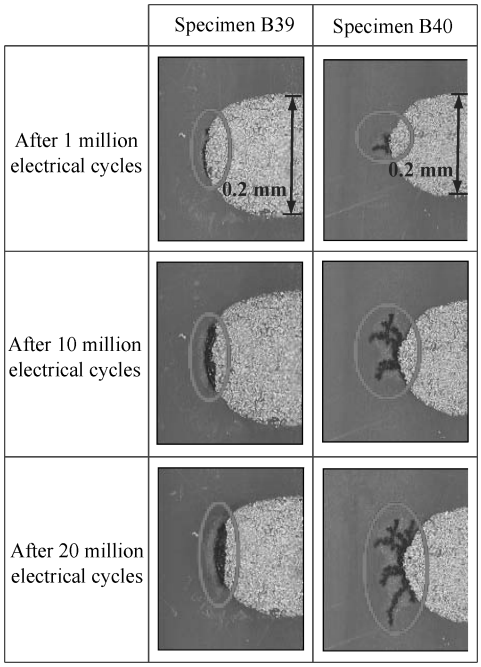

Fig. 10 Electrical fatigue burns underneath electrode fingertips.

generated from the rapid variation of the high electric field between the fiber and the electrode. Once a burn was initiated, the charring created a conductive material, which in turn increased the electric field by reducing the effective distance between the fiber and the electrode. This was a compounding process that made fatigue burns grow with the number of electrical cycles. The burning between the fiber and the electrode made them grow along the electrode finger and not from one finger to the adjacent finger.

Even though electrical fatigue did not cause immediate problems during the life of the AMR blade tests, this type of compounding burning process made it possible for the burns to grow up to the adjacent electrode finger with the opposite polarity, to cause catastrophic electrical failure at very high electrical fatigue levels. Such fatigue burns could lead to potential limitation in the actuator material system during long-term operation of AFC embedded rotor

blades in a production application. Therefore, further improvements to the AFC material system must be considered in future material developments to address the issue of electrical fatigue burns at high-frequency actuation conditions.

Mechanical Fatigue Tests

The mechanical fatigue tests were designed to simulate the repeated mechanical loading on the embedded AFC actuators during the AMR blade operation. Mechanical fatigue on AFCs may lead to deterioration in actuation performance, reduction in modulus, complete loss of actuation due to electrical failure, or even catastrophic mechanical failure. Therefore, it was very important to evaluate the ability of the AFC material system to operate reliably under high mechanical fatigue conditions while sustaining actuation performance and maintaining mechanical strength.

Test Articles

Baseline AFC actuator coupons shown in Fig. 4 were symmetrically laminated with E–glass to perform tests under mechanical fatigue. The laminated configuration was chosen to replicate the active composite structure of the AMR blade to understand the effect of the passive structure in the AFC mechanical fatigue behavior. The high-voltage wires were attached to the silver electrode tabs with silver-based conductive epoxy (VonRoll Isola USA, Inc., Schenectandy, New York). The loading tabs necessary to grip the specimen on the tensile testing machine were bonded over the electrode tabs with a high-strength adhesive film (McMaster–Carr Supply, New Bruncwick, New Jersey). Model WD-DY-125AD-350 unidirectional strain gagues (Micro-Measurements, Raleigh, North Carolina) rated for high mechanical fatigue were bonded using M-Bond 610 on both sides of the E–glass laminated specimens to measure both the mechanical strain and the induced actuation strain of the specimen. An actuator coupon prepared for mechanical fatigue testing is shown in Fig. 11.

Test Setup and Procedure

A servohydraulic tensile testing machine (Instron Corporation, Canton, Massachusetts) with hydraulic grips was used in "load control" mode to apply the repetitive mechanical loading to the AFC specimen. The mechanical load on the specimen corresponding to the required mechanical strain cycle was set at the beginning of the test. Accordingly, a permanent strain or a reduction in stiffness lead to higher mechanical strains. The test setup in Fig. 12 shows the servohydraulic test machine and the associated equipment used for the mechanical fatigue tests. The data acquisition computer recorded the load and stroke data from the Instron machine, applied voltage from the amplifier, and strain data from the strain gauge conditioners.

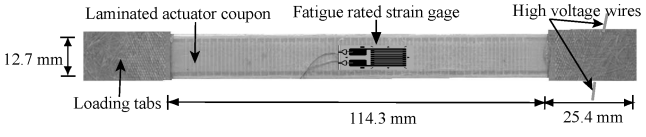

Fig. 11 Actuator coupon prepared for mechanical fatigue tests.

The actuators were tested under mechanical fatigue using two fatigue load levels. Initially, the specimens were tested under the nominal fatigue load corresponding to a sinusoidal mechanical strain cycle of $1000 \pm 900\ \mu\varepsilon$. This nominal fatigue load level was selected to represent the operational loads expected during the AMR blade operation. After completing the nominal fatigue test, the same specimens were tested again at a 50% higher fatigue load level. This extended fatigue load corresponds to a strain cycle of $1500 \pm 1350\ \mu\varepsilon$. The extended loading cycle fatigue test was conducted to determine the fatigue limit of the AFC material system at higher cyclic strain.

The tests were run at 23-Hz frequency to simulate the 1 per revolution mechanical loading condition expected in the AMR blade operation. The actuators were tested up to 10 million mechanical cycles or to catastrophic mechanical failure in accordance to the the American Society for Testing and Materials D3479 standard.[22] The total duration for a 10 million cycle fatigue test at 23 Hz was approximately 6 days. During the fatigue test, the longitudinal modulus of the specimen was measured at logarithmic cycle intervals by conducting a load/unload cycle on the specimen. Loading/unloading rate of 5 N/s was used to maintain a quasi-static condition to eliminate rate effects in the modulus measurement.

The induced strain performance of the actuator was also measured at corresponding mechanical cycle intervals by applying a customized driving electrical cycle. This driving voltage was a 3000-Vpp sinusoidal cycle with 0 Vdc at 1 Hz generated by the LabVIEW software. The voltage cycle was customized to apply five sinusoidal cycles to the actuator and two 0-V segments at the beginning and end of the sinusoidal segment. The strain gauge data acquired during the initial 0-V segment measured the static mechanical strain on the test specimen to determine any permanent strain. The 0-V segment at the end of the cycle ensured that the actuator electrical condition was reset to a short circuit before the next mechanical cycle. It was not suitable to strain the actuator mechanically with an open-circuit electrical condition because this generated an electrical field within the piezoceramic fibers. The details of the electromechanical testing sequence along with the customized driving voltage cycle used for mechanical fatigue test are shown in Fig. 13.

The strain data from gauges on both sides of the specimen were averaged to calculate the mechanical strain and the induced actuation strain. The induced strain performance was determined by taking the difference between the maximum and the minimum strains measured during the sinusoidal segment of the voltage function. The chord modulus of the specimens was calculated for the mechanical strain range from 100 to 2000 $\mu\varepsilon$. The AFC modulus was calculated in terms of strain ranges to capture the high nonlinearity of the AFC material system. Using the modulus data of the E–glass laminated specimen, the resultant longitudinal modulus from the AFC inside the laminate was indirectly extracted by analytically removing the contribution of E–glass. This was calculated using a mechanics of material model of the laminate and the corresponding modulus of pure E–glass.[23] Note that fatigue tests conducted on pure [0-deg/90-deg] cross ply E–glass specimen at nominal and extended mechanical fatigue load levels indicated no degradation in

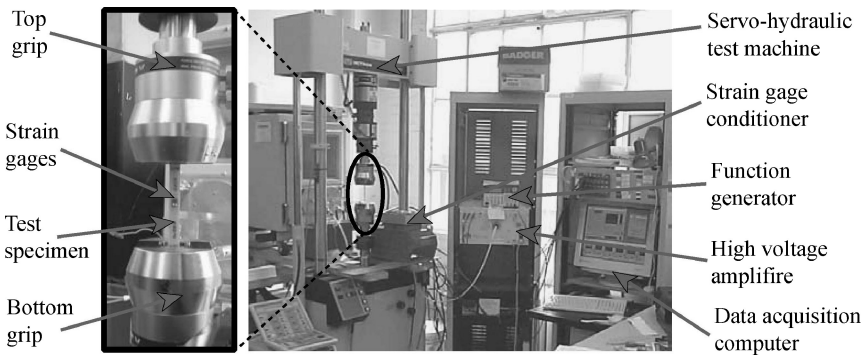

Fig. 12 Mechanical fatigue test setup with servohydraulic tensile testing machine.

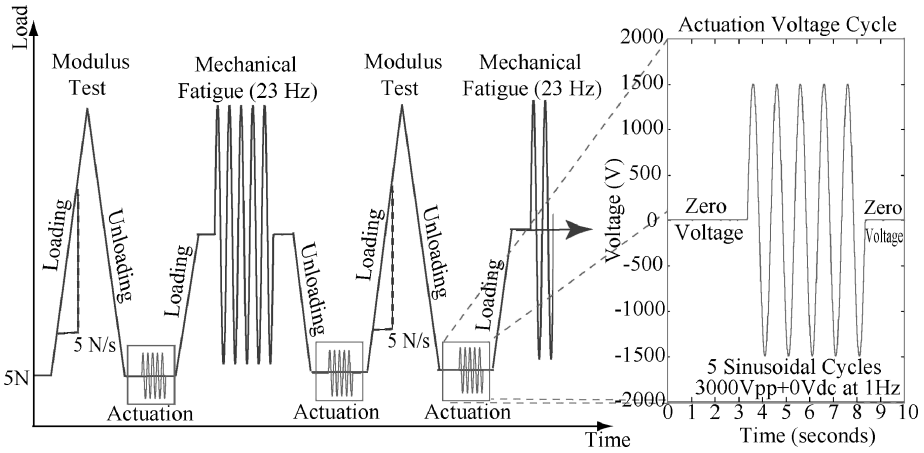

Fig. 13 Mechanical fatigue testing sequence and applied driving voltage cycle.

Table 2 Summary of mechanical fatigue specimen performance and test conditions

Specimen	Fatigue loads $\mu\varepsilon$	Initial modulus, GPa	Initial actuation, $\mu\varepsilon$
B27	1000 ± 900	25	692
B27	1500 ± 1350	23	678
B42	1000 ± 900	20	348
B42	1500 ± 1350	20	345

modulus up to 10 million cycles. Therefore, modulus degradation in the laminated AFC specimens was likely due to the deterioration in the AFC modulus.

Test Results

The mechanical fatigue tests performed on the actuator coupons provided an invaluable insight into the AFC behavior under dynamic mechanical loading conditions. The actuator coupon B27 was symmetrically laminated with one ply of E–glass, whereas the specimen B42 was symmetrically laminated with two plies of E–glass. The test conditions along with the initial actuation and the initial extracted AFC chord modulus for 100–2000 $\mu\varepsilon$ is summarized in Table 2.

The variation in the actuation during the test, normalized by the initial actuation measured after the first loading cycle, is shown in Fig. 14. The normalized AFC chord modulus vs the number of mechanical cycles is shown in Fig. 15. The measured modulus was normalized by the initial modulus to facilitate the comparison of actuators with two levels of E–glass lamination.

Both actuator coupons tested under the nominal fatigue load level of 1000 ± 900 $\mu\varepsilon$ up to 10 million cycles showed no degradation in induced strain performance or reduction in modulus, as shown in Figs. 14 and 15, respectively. This confirmed that the AFC actuators would survive the dynamic mechanical fatigue conditions expected in the AMR blade operational environment. Relatively constant level of actuation and modulus observed during these tests indicated that the AFC actuators would not sustain observable damage during the nominal mechanical fatigue condition.

After completing the fatigue test at the nominal load level, the actuators were mechanically fatigued at a 50% higher load corresponding to a strain cycle of 1500 ± 1350 $\mu\varepsilon$. During the extended fatigue tests, the actuator coupon B27 symmetrically laminated with a single ply of E–glass suffered two-part failure shortly after 7 million cycles. The specimen B27 showed a gradual degradation in modulus and actuation after 5 million cycles. However, the level of constraint with a single ply of E–glass was much lower than the constraint level expected in the AMR blade actuators due to the surrounding passive structure. In contrast, under a similar extended fatigue loading condition, the actuator coupon B42 symmetrically laminated with two plies of E–glass showed no degradation in modulus or actuation up to 10 million cycles. Lamination with two plies of E–glass more accurately represented the constraint condition in the blade actuators.

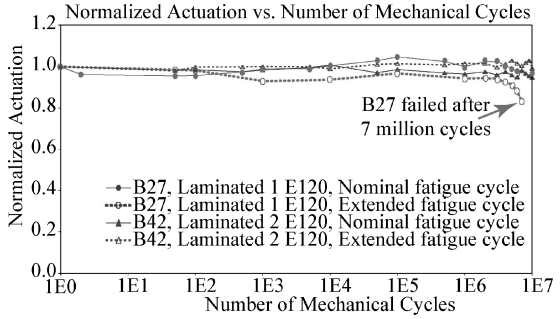

Fig. 14 Actuation performance variation during mechanical fatigue tests.

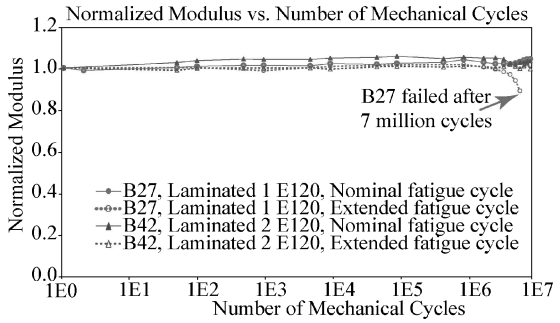

Fig. 15 Chord modulus variation during mechanical fatigue tests.

Therefore, the fatigue tests at extended load level further demonstrated the high robustness qualities of the AFC material system under mechanical fatigue. Such long-term durability was essential to employ AFCs successfully as structural actuators in the AMR blade application.

Conclusions

This study was conducted to characterize the long-term durability performance of the AFC actuator material system for the Boeing AMR blade application. The preliminary characterization tests designed to extract the important electromechanical durability properties under simulated blade operating conditions were mechanical fatigue tests and electrical fatigue tests.

The AFC material system characterized for the AMR blade application consisted of 0.25-mm-diam PZT-5A fibers embedded in a dry film matrix. The AFC material system exhibited hysteresis in actuation and the average induced strain performance of an unlaminated actuator was 1200 $\mu\varepsilon$ for 3000 Vpp with 0 Vdc, the optimum voltage cycle selected for the blade operation. The longitudinal chord modulus in a baseline actuator for the strain range of 100–2000 $\mu\varepsilon$ was 26 GPa.

Electrical fatigue tests were conducted to simulate the repeated actuation of AFCs during the blade operation. Actuators tested up to 20 million electrical cycles showed no degradation in induced strain performance. However, microscopic inspection showed evidence of damage in the form of fatigue burns, but none of the burns were large enough to cause catastrophic electrical failure in the actuator.

Mechanical fatigue tests were conducted to simulate the repeated mechanical loading on actuators during the blade operation. E–glass laminated actuators tested to 10 million cycles at the nominal load level of $1000 \pm 900\ \mu\varepsilon$ showed no significant deterioration in the modulus or actuation capability. An actuator coupon that corresponded to the lamination level expected in the AMR blade actuators retained the stiffness and performance properties even after additional 10 million cycles at a 50% higher fatigue load level.

The results of this comprehensive long-term durability characterization of the AFC material system supported the design and operation of the Boeing AMR blades scheduled for wind-tunnel tests. The test results were used to understand and to predict the electromechanical behavior and performance of the AFC actuator in blade operating conditions. Furthermore, this study developed a viable testing methodology for efficient evaluation of the durability properties of active material actuators for future structural application development.

Acknowledgments

Funding for this research was provided by the Defense Advanced Research Projects Agency under the Phase II of the Smart Materials and Structures Demonstration Consortium and was monitored by Ephrahim Garcia of the Defense Sciences Office. This project was continuously supported by Douglas Weems and Robert Derham at The Boeing Company, Philadelphia as well as Alex Pizzochero and Aaron Bent at Continuum Control Corporation. Special thanks are extended to colleagues at Active Materials and Structures Laboratory (AMSL)—Massachusetts Institute of Technology and Institute for Aerospace Research (IAR)—National Research Council Canada.

References

[1]Kretz, M., and Larche, M., "Future of Helicopter Rotor Control," *Vertical*, Vol. 4, Spring 1980, pp. 13–22.

[2]Lemnios, A. Z., Smith, A. F., and Nettles, W. E., "The Controllable Twist Rotor Performance and Blade Dynamics," *Proceedings of the 28th Annual National Forum of the American Helicopter Society*, American Helicopter Society Publications Dept., Alexandria, VA, 1972.

[3]Prechtl, E. F., and Hall, S. R., "Closed-Loop Vibration Control Experiments on a Rotor with Blade Mounted Actuation," AIAA Paper 2000-1714, April 2000.

[4]Straub, F. K., Ngo, H. T., Anand, V., and Domzalski, D. B., "Development of a Piezoelectric Actuator for Trailing Edge Flap Control of Full Scale Rotor Blades," *Journal of Smart Materials and Structures*, Vol. 10, No. 1, 2001, pp. 25–34.

[5]Rodgers, J. P., and Hagood, N. W., "Hover Testing of 1/6 Mach-Scale CH-47D Blade with Integral Twist Actuation," *Proceedings of the 9th International Conference on Adaptive Structures and Technology*, Cambridge, MA, 1998.

[6]Shin, S. J., and Cesnik, C. E. S., "Forward Flight Response of the Active Twist Rotor for Helicopter Vibration Reduction," AIAA Paper 2001-1357, Seattle, WA, April 2001.

[7]Chen, P. C., and Chopra, I., "Induced Strain Actuation of Composite Beams and Rotor Blades with Embedded Piezoceramic Elements," *SPIE Smart Structures and Intelligent Systems Conference*, Vol. 2190, International Society for Optical Engineering, Bellingham, WA, 1994, pp. 123–140.

[8]Derham, R. C., and Hagood, N. W., "Rotor Design Using Smart Materials to Actively Twist Blades," *Proceedings of the 52nd Annual Forum of the American Helicopter Society*, American Helicopter Society Publications Dept., Alexandria, VA, 1996.

[9]Hagood, N. W., and Pizzochero, A., "Residual Stiffness and Actuation Properties of Piezoelectric Composites: Theory and Experiment," *Proceedings of the 9th International Conference on Adaptive Structures and Technology*, Cambridge, MA, 1998.

[10]Rodgers, J. P., Bent, A. A., and Hagood, N. W., "Characterization of Interdigitated Electrode Piezoelectric Fiber Composites Under High Electrical and Mechanical Loading," *Proceeding of the SPIE Annual International Symposium on Smart Structures and Materials*, Vol. 2717, The International Society for Optical Engineering, Bellingham, WA, 1996, pp. 642–659.

[11]Schmidt, M. C., and Hagood, N. W., "Design and Manufacturing of a Second Generation Integral Twist-Actuated Rotor Blade," AIAA Paper 2000-1710, April 2000.

[12]Derham, R. C., Matthew, B., and Weems, D. B., "An Introduction to the Aeromechanical Design Space of 'Smart' Rotors," American Helicopter Society Northeast Region National Specialists' Meeting: Improving Rotorcraft Acceptance through Active Controls Technology, Oct. 2000.

[13]Mall, S., and Coleman, J. M., "Monotonic and Fatigue Loading Behavior of Quasi-Isotropic Graphite/Epoxy Laminate Embedded with Piezoelectric Sensor" *Journal of Smart Materials and Structures*, Vol. 6, No. 6, 1998, pp. 822–832.

[14]Wickramasinghe, V. K., and Hagood, N. W., "Performance Characterization of Active Fiber Composite Actuators for Helicopter Rotor Blade Applications," *Proceeding of the 9th SPIE Annual International Symposium on Smart Structures and Materials*, Vol. 4699, Society of Photo-Optical Instrumentation Engineers, Bellingham, WA, 2002, pp. 273–284.

[15]Ghandi, K., "Non-Linear Modeling and Characterization Techniques for Phase Transitions in Electromechanically Coupled Devices," Ph.D. Dissertation AMSL No. 98-1, Dept. of Aeronautics and Astronautics, Massachusetts Inst. of Technology, Cambridge, MA, May 1998.

[16]Bent, A. A., and Hagood, N. W., "Improved Performance in Piezoelectric Fiber Composites Using Interdigitated Electrodes," *Proceedings of the SPIE Smart Structures and Materials Conference*, Vol. 2441, The International Society for Optical Engineering, Bellingham, WA, 1995, pp. 196–212.

[17]Jaffe, B., Cook, W. R., and Jaffe, H., *Piezoelectric Ceramics*, Academic Press, New York, 1971.

[18]Strock, H. B., Pascucci, M. R., Parish, M. V., Bent, A. A., and Shrout, T. R., "Active PZT Fibers, A Commercial Production Process," *Proceeding of the 6th SPIE Annual International Symposium on Smart Structures and Materials*, Vol. 3675, Society of Photo-Optical Instrumentation Engineers, Bellingham, WA, 1999, pp. 22–31.

[19]Berlincourt, D., "Piezoelectric Crystals and Ceramics," *Ultrasonic Transducer Materials*, edited by O. E. Mattiat, New York, 1971, Chap. 2, pp. 63–121.

[20]Jones, R. M., *Mechanics of Composite Materials*, Taylor and Francis, Philadelphia, 1999.

[21]Bent, A. A., Hagood, N. W., and Rodgers, J. P., "Anisotropic Actuation with Piezoelectric Fiber Composites," *Journal of Intelligent Material Systems and Structures*, Vol. 6, No. 3, 1995, pp. 338–349.

[22]"Standard Test Method for Tensile-Tension Fatigue of Oriented Fiber Resin Matrix Composites," ASTM D3479, Vol. 15.03, American Society for Testing and Materials, Conshohocken, PA, 1995, pp. 148–150.

[23]Wickramasinghe, V. K., "Characterization of Active Fiber Composites Actuators for Helicopter Rotor Blade Applications," M.S. Thesis, AMSL No. 01-02, Dept. of Aeronautics and Astronautics, Massachusetts Inst. of Technology, Cambridge, MA, March 2001.